Generation of coherent optical multi-carriers using concatenated, dual-drive Mach-Zehnder and phase modulators

Shumin Zou (邹书敏), Yiguang Wang (王一光), Yufeng Shao (邵宇丰), Junwen Zhang (张俊文), Jianjun Yu (余建军), and Nan Chi (迟 楠)*

State Key Laboratory of ASIC and System, Department of Communication Science and Engineering, Fudan University, Shanghai 200433, China

**Corresponding author: nanchi@fudan.edu.cn*

Received November 8, 2011; accepted January 18, 2012; posted online March 31, 2012

The generation of coherent optical subcarriers based on a concatenated dual-drive Mach-Zehnder intensity modulator (IM) and two phase modulators (PMs) is proposed and experimentally demonstrated. The modulation index and DC bias of PM+IM modulation are theoretically investigated. Theoretical analysis and numerical study are also carried out to examine the proposed scheme. We use 25-GHz RF synchronous sinusoidal signals to drive cascaded two-stage PMs and IM, through which we generate 28 subcarriers with peak power fluctuations less than 4 dB. The measured tone-to-noise ratio of the subcarrier is higher than 40 dB. The experimental results show that for 100-Gb/s polarization multiplexing QPSK signal, the receiver sensitivity of the back-to-back signal is −28.6 dBm, and the power penalty is lower than 1 dB after 100-km transmission at the BER of 1×10^{-9}.

OCIS codes: 060.1660, 060.2330, 060.2380.
doi: 10.3788/COL201210.070605.

The bandwidth demands for communication and computer applications have grown in recent years, such as in the areas of Internet video applications, downloads, and so on; thus, it has become necessary for optical communication to migrate from 10 to 100 Gb/s or even higher (e.g., 1 Tb/s)[1−8]. Given that wavelength-division-multiplexing (WDM)[5,6] and coherent optical frequency-division multiplexing (OFDM)[7−9] are promising techniques for such high-speed long-haul transmissions, many researchers have attempted to come up with better techniques to achieve high-speed transmission. Recently, a 16×112 Gb/s NRZ-DQPSK modulation format for dense WDM (DWDM) transmission[6] and a 1.2-Tb/s orthogonal DWDM transmission[10] have been reported. To increase the capacity of WDM transmission, many approaches have been proposed, such as expanding the usable wavelength band, increasing the bit rate, narrowing the channel spacing[11], using new optical fibers, and compensating for nonlinearities. With these approaches, a multi-carrier transmission system with narrower channel spacing (i.e., increased spectral efficiency) is suitable for long haul transmission, because it can decrease the bit rate of every single channel with large number of multi-wavelengths. However, the key research issue for multi-wavelength transmission, i.e., the source should be stable, compact, and cost-effective, must be addressed.

There are several techniques to generate multi-carriers. First of these is the supercontinum (SC) generation, which is the combination of an optical pulse generator and nonlinear fiber. In this method, the optical pulse spectrum is broadened based on optical pulse compression through a nonlinear fiber[12,13]. The second technique is a combination of a periodically driven Mach-Zehnder modulator (MZM) and a nonlinear fiber. Here, CW light is periodically amplitude modulated and then coupled to a nonlinear fiber, in which the light undergoes additional modulation by the process of self-phase modulation[14]. The third method features concatenated Mach-Zehnder (MZ) intensity modulator (IM) and phase modulators (PMs) comprising a simple configuration based on a hybrid sinusoidal amplitude-phase modulation using tandem $LiNbO_3$ modulators[15−17]. The fourth method is a combination of an optical single-sideband (SSB) modulator and an optical fiber loop; here, the SSB modulator shifts the frequency of the optical signal to generate multiple combs sequentially each time the lightwave circulates in the loop[8,18,19]. However, the above techniques suffer from low OSNR (which is less than 25 B), as well as a low number of generated subcarriers that are less than 20, within a 2-dB power variation and amplitude fluctuation around 5 dB.

In this letter, we theoretically investigate the operating mechanism of a multi-wavelength generation method based on a concatenated dual-drive MZM and PM. Theoretical analysis and numerical study are carried out, and 25-GHz RF synchronous sinusoidal signals are used to drive the cascaded two-stage PMs and IM, through which we generated 28 subcarriers with peak power fluctuation less than 4 dB. The measured tone-to-noise ratio of the subcarrier is higher than 40 dB. The experimental results show that for 100-Gb/s polarization multiplexing QPSK signal, the receiver sensitivity of the back-to-back (BTB) signal is −28.6 dBm, and the power penalty is lower than 1 dB after 100-km transmission at the BER of 1×10^{-9}. Experimental results demonstrate the successful generation of multi-subcarriers for high-speed transmission.

With the input optical signal as $E_{\rm in}(t) = A\cdot\exp(\mathrm{j}2\pi f_{\rm o}t)$, and the RF drive signal as $V_{\rm r1}(t) = V_1\sin(2\pi f_1 t)$, the transfer function of phase modulator

is given by

$$E_{\rm out} = E_{\rm in}(t)\exp\left(\mathrm{j}\pi\frac{V_{\rm d}}{V_\pi}\right) = E_{\rm in}(t)\exp[\mathrm{j}\pi R_1\sin(2\pi f_{\rm s}t)], \quad (1)$$

where V_π is half-wave voltage of PM, and $R_1 = \frac{V_1}{V_\pi}$ is the phase modulation depth. If there are N PMs cascaded, we can obtain

$$\begin{aligned} E_{\rm out}(t) &= E_{\rm in}(t)\exp[\pi R_1\sin(2\pi f_{\rm s}t)] \\ &\cdot \exp[2\pi R_2\sin(2\pi f_{\rm s}t)]\cdots[2\pi R_n\sin(2\pi f_{\rm s}t)] \\ &= E_{\rm in}(t)\exp[\pi(R_1+R_2+\cdots R_n)\sin(2\pi f_{\rm s}t)] \\ &= E_{\rm in}(t)\exp[\pi(R_N)\sin(2\pi f_{\rm s}t)], \end{aligned} \quad (2)$$

where $R_N = R_1 + R_2 + \cdots + R_n$, and the effect of cascaded N PMs can be seen as that of one PM. Thus, for simplicity, we used one phase modulator to replace the cascaded PMs for the following analysis.

When using the Jacobi-Anger expansion, Eq. (1) can be expressed as

$$E_{\rm out}(t) = E_{\rm in}(t)\sum_{n=-\infty}^{\infty} J_n(\pi R_1)\exp(\mathrm{j}2\pi n f_{\rm s}t). \quad (3)$$

Thus, the output power of kth subcarrier is

$$P_k = E_k\cdot\overline{E}_k = [E_{\rm in}(t)J_k(\pi R_1)]^2\exp(\mathrm{j}2\pi k f_{\rm s}t) \cdot\exp(\mathrm{j}2\pi k f_{\rm s}t) = E_{\rm in}^2(t)J_k(\pi R_1)^2. \quad (4)$$

From Eq. (4), the output power of the kth subcarrier is dedicated by the phase modulation depth R_1, when $E_{\rm in}(t)$ is unchanged. As such, the number of subcarriers within a given target amplitude increases when R_1 increases. In order to obtain large R_1, we can cascade more PMs; Eq. (2) proves that cascaded modulators are equivalent to using one modulator. In our experiment, we cascaded two PMs. However, due to the gap in output power between different order subcarriers, we used a MZ IM to decrease the power difference between the subcarriers within a given target amplitude.

The MZ IM we used had a typical arm (upper and lower) and dual (separate DC and RF) electrode configuration. The transfer function of the IM is

$$\begin{aligned} E_{\rm out}(t) &= \frac{E_{\rm in}(t)}{2}\left[\exp\left(\frac{\mathrm{j}\pi V_{\rm lower}}{V_{\pi\rm rf}}+\frac{\mathrm{j}\pi V_{\rm dc}}{V_{\pi\rm dc}}\right)+\exp\left(-\frac{\mathrm{j}\pi V_{\rm upper}}{V_{\pi\rm rf}}\right)\right] \\ &= \frac{E_{\rm in}(t)}{2}\{\exp[\mathrm{j}\pi R_2\sin(2\pi f_{\rm s}t)+\mathrm{j}\pi D] \\ &+ \exp[-\mathrm{j}\pi R_2\sin(2\pi f_{\rm s}t)]\}, \end{aligned} \quad (5)$$

where $V_{\pi\rm rf}$ is the half-wave voltage of the RF signal; $V_{\pi\rm dc}$ is the half-wave voltage of DC signal; $V_{\rm lower}$ and $V_{\rm upper}$ are the input RF signals, where $V_{\rm lower} = V_{\rm upper} = V_2\sin(2\pi f_{\rm s}t)$ in this case; $R_2 = \frac{V_2}{V_{\pi\rm rf}}$ is the phase modulation depth; $V_{\rm dc}$ is the input DC bias of lower arm, $D = \frac{V_{\rm dc}}{V_{\pi\rm dc}}$.

Figure 1 shows the configuration of a multi-wavelength generator comprising a tunable semiconductor laser diode (TLD), two PMs, a dual-drive MZ IM, two phase shifters, two RF signals, and three microwave amplifiers.

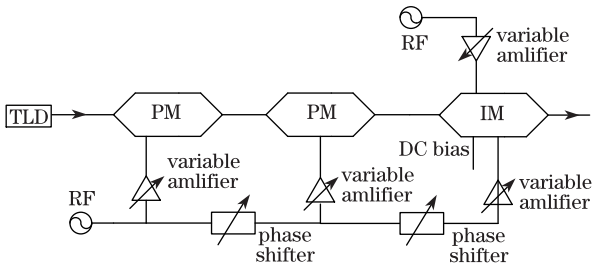

Fig. 1. Principle of multi-subcarrier generation.

The CW light was inputted into the modulators and modulated by sinusoidal electrical signals that were then applied to the PMs and IM. In the previous analysis, the transfer function of the cascaded PMs can be seen as that of one PM; thus, the electrical field of two PMs and a single IM at the output is given by

$$\begin{aligned} E_{\rm out} &= E_{\rm in}(t)\exp[\mathrm{j}\pi R_1\sin(2\pi f_{\rm s}t)]\{\exp[\mathrm{j}\pi R_2\sin(2\pi f_{\rm s}t)+\mathrm{j}\pi D] \\ &+ \exp[-\mathrm{j}\pi R_2\sin(2\pi f_{\rm s}t)]\} \\ &= E_{\rm in}(t)\{\exp(\mathrm{j}\pi D)\cdot\exp[\mathrm{j}\pi(R_1+R_2)\sin(2\pi f_{\rm s}t)] \\ &+ \exp[\mathrm{j}\pi(R_1-R_2)\sin(2\pi f_{\rm s}t)]\}. \end{aligned} \quad (6)$$

When using the Jacobi-Anger expansion, Eq. (6) can be expressed as

$$\begin{aligned} E_{\rm out} = E_{\rm in}(t)\Big\{&\exp(\mathrm{j}\pi D)\cdot\sum_{n=-\infty}^{\infty} J_{\rm n}[\pi(R_1+R_2)]\exp(\mathrm{j}2\pi n f_{\rm s}t) \\ &+ \sum_{n=-\infty}^{\infty} J_{\rm n}[\pi(R_1-R_2)]\exp(\mathrm{j}2\pi n f_{\rm s}t)\Big\}. \end{aligned} \quad (7)$$

From Eq. (7), the kth-order subcarrier is

$$\begin{aligned} E_k = E_{\rm in}(t)\{&J_k[\pi(R_1+R_2)]\exp(\mathrm{j}2\pi k f_{\rm s}t+\mathrm{j}\pi D) \\ &+ J_k[\pi(R_1-R_2)]\exp(\mathrm{j}2\pi k f_{\rm s}t)\}. \end{aligned} \quad (8)$$

When $|\arg A| < \pi$, the Bessel series is approximately given by

$$J_k(A) = \sqrt{\frac{2}{\pi A}}\left[\cos\left(A-\frac{1}{2}k\pi-\frac{1}{4}\pi\right)+\mathrm{e}^{|\phi_A|}O(|A|^{-1})\right](|\arg A|<\pi), \quad (9)$$

whereas when $|\arg[\pi(R_1+R_2)]| < \pi$ and $|\arg[\pi(R_1-R_2)]| < \pi$, Eq. (8) is approximately shown as

$$\begin{aligned} E_k &\approx E_{\rm in}(t)\sqrt{\frac{2}{\pi\overline{A}}}\left\{\begin{array}{l}\cos\left(A_1-\frac{1}{2}k\pi-\frac{1}{4}\pi+O(A_1^{-1})\right) \\ \cdot\exp(\mathrm{j}2\pi k f_{\rm s}t+\mathrm{j}\pi D)+ \\ \cos\left(A_2-\frac{1}{2}k\pi-\frac{1}{4}\pi+O(A_2^{-1})\right) \\ \cdot\exp(\mathrm{j}2\pi k f_{\rm s}t)\end{array}\right\} \\ &= E_{\rm in}(t)\sqrt{\frac{2}{\pi\overline{A}}}\left\{\begin{array}{l}\cos\left(\overline{A}-\frac{(2k+1)}{4}\pi+\Delta A+O(\overline{A}^{-1})\right) \\ \cdot\exp(\mathrm{j}2\pi k f_{\rm s}t+\mathrm{j}\pi D)+ \\ \cos\left(\overline{A}-\frac{(2k+1)}{4}\pi-\Delta A+O(\overline{A}^{-1})\right) \\ \cdot\exp(\mathrm{j}2\pi k f_{\rm s}t)\end{array}\right\}, \end{aligned} \quad (10)$$

where $A_1 = \pi(R_1 + R_2)$, $A_2 = \pi(R_1 - R_2)$, $\overline{A} = \frac{A_1+A_2}{2}$, $\Delta A = \frac{A_1-A_2}{2}$, and $Q = \overline{A} - \frac{(2k+1)}{4}\pi + O(\overline{A}^{-1})$.

The ratio of the kth subcarrier to the input optical power is given by

$$\begin{aligned}\eta_k &= \frac{P_k}{P_{\text{in}}} \\ &= \cos(Q+\Delta A)^2 + \cos(Q-\Delta A)^2 \\ &\quad + 2\cos(Q+\Delta A)\cos(Q-\Delta A)\cos(\pi D) \\ &= 1 + \cos(\pi D)\cos(2\Delta A) + [\cos(\pi D) + \cos(2\Delta A)] \\ &\quad \cdot \cos\left(2\overline{A} - \frac{(2k+1)}{2}\pi + 2O\left(\overline{A}^{-1}\right)\right). \end{aligned} \tag{11}$$

Ignoring the extinction ratio and insertion loss, the power conversion efficiency is almost constant and independent of the order of the subcarriers when $\cos(\pi D)+\cos(2\Delta A)=0$, $2\Delta A = \pi D + (2k+1)\pi$, $(k = 0, \pm1, \pm2\cdots)$. Meanwhile, $\Delta A = \frac{A_1-A_2}{2} = \frac{\pi(R_1+R_2)-\pi(R_1-R_2)}{2} = \pi R_2$,

$$R_2 - \frac{D}{2} = \frac{1}{2} + k, \quad k = 0, \pm1, \pm2, \cdots. \tag{12}$$

This means that theoretically, the subcarriers are flat when the difference between the phase modulation depth and DC modulation depth of the IM is $1/2+k$.

Aside from the theoretical analysis, we performed two simulation experiments, namely, VPI simulation and Matlab, to find out the optimum points for multi-subcarriers and demonstrate the effectiveness of the proposed technique.

First, we conducted a simulation to obtain the optimal operation point for five subcarriers using a single IM[20]. The simulation layout comprised a single 1 553.6-nm CW laser and an ideal MZ IM. The half-wave voltage of DC bias ($V_{\pi\text{dc}}$) was 2 V, and the half-wave voltage of the RF drive ($V_{\pi\text{rf}}$) was 4 V. We changed the DC bias from 3 to 4 V and the RF drive voltage (V_{rf}) from 1.5 to 2 V for further simulation. Figure 2 shows the calculated natural logarithmic of the variance fluctuations of the five tones with the DC bias and RF drive voltage of the MZM. A higher natural logarithmic means that the variance is smaller and the five tones are smoother and steadier; we then obtained the following optimum

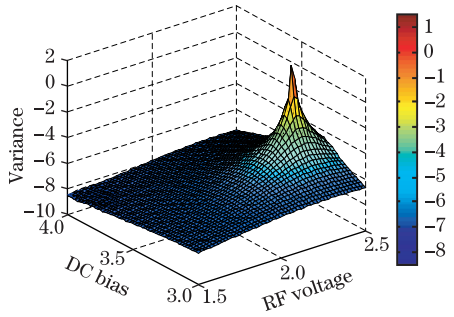

Fig. 2. Contour plot of the calculated variance as functions of the DC bias and the RF voltage.

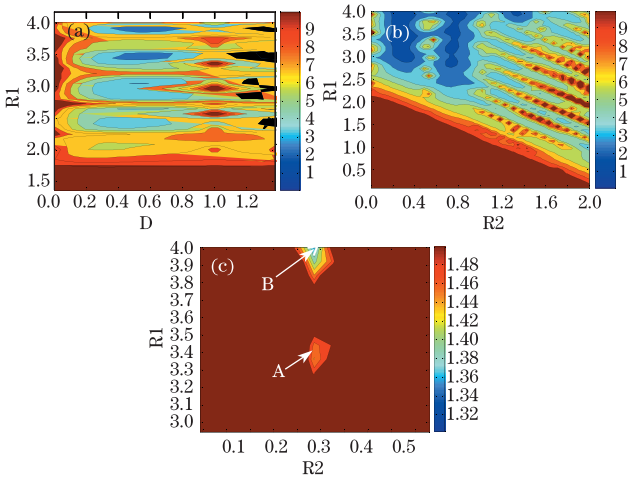

Fig. 3. Variances of 22 subcarriers versus (a) IM DC bias and PM phase modulation index and (b) PM phase modulation index and IM phase modulation index, and (c) detailed configuration of (b).

points from the simulation result: V_{dc} is 3.36 V and V_{rf} is 2.35 V, $D = \frac{V_{\text{dc}}}{V_{\pi\text{dc}}}$=1.68, and RF drive modulation index is 0.5875.

Next, we simulated the proposed multi-subcarrier generation with concatenated dual-drive MZ IM and PM. The simulation comprises one 1 550-nm CW laser with 1-mW output power and 1-MHz linewidth. As in the previous analysis, the transfer function of the two cascaded PMs can be seen as that of one PM and one ideal MZM as shown in Eq. (6). PM and MZ IM are driven by 25-GHz RF clocks, and the MZM is driven by 25-GHZ RF clocks; the initial phase of the 25-GHz clock is zero, and the voltages of two RF signals are both 3.8 V.

Considering the experiment condition, we adjusted the R_1 value range (from 0 to 4) of the PM RF signals in the simulation. We set R_2 to 0.5 and obtained the peak power (in the declined 5 dB range) of the 27 subcarriers when we changed D from 0 to 2 and R_1 from 0.1 to 4, respectively. Then we calculated the peak power variance of the 27 subcarriers as shown in Fig. 3(a). It shows that when D is around 0.5, the power variance of 27 subcarriers is minimal. Then, we set D to 0.5 and change R_1 from 0.1 to 4 and R_2 from 0 to 2. The simulation result is shown in Fig. 3(b), and as can be seen, the power variances are low in an area when R_1 is above 3 and when R_2 is between 0.2 to 0.4. In order to produce more accurate results, we changed R_1 from to 4 and R_2 from 0.05 to 0.5. The detailed result is shown in Fig. 3(c), and as can be seen, there are two optimum points: point A, where R_1 is equal to 3.35 and R_2 is equal to 0.286, and point B, in which R_1 is equal to 4 and R_2 is equal to 0.286.

Figure 4 is the simulation diagram of the optical spectrum of the two optimum points. Figure 4(a) is the optical spectrum of point A, and Fig. 4(b) is the optical spectrum of point B. Given that the optical spectrum of point B is flatter than that of point A, we take the former's value to generate 22 subcarriers using the proposed multi-carrier technique.

The experimental setup for multi-subcarriers generation is shown in Fig. 5. The CW lightwave at 1 557.80 nm

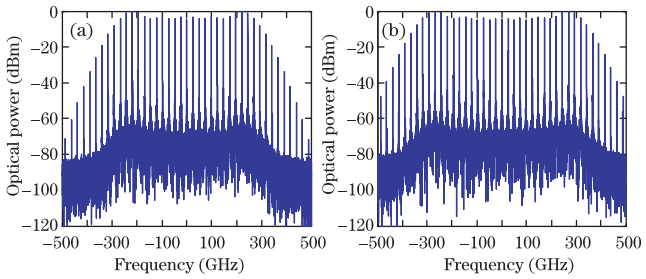

Fig. 4. Simulation optical spectra of points (a) A and (b) B.

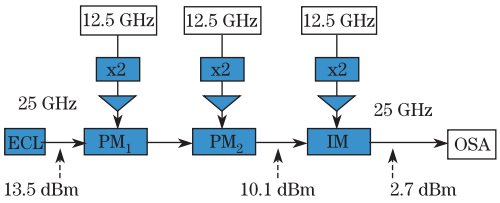

Fig. 5. Experimental setup. OSA: optical spectrum analyzer.

generated by one external cavity laser (ECL) with an output power of 13.5 dBm was modulated using two cascaded PMs and one MZ IM; both demonstrated identical electro-optical performance when the DC bias and the RF voltage of the MZM were carefully selected. Next, we used three independent frequency multipliers to produce three 25-GHz RF signals, after which these RF signals were adopted to drive each modulator. Then, booster electrical amplifiers were used to produce large amplitude RF signals (the voltages of the two RF signals were both 3.8 V). The PMs (PM_1 and PM_2) had a small insertion loss of about 3.4 dB as shown in Fig. 5. In comparison, the MZ IM had high insertion loss of about 7.4 dB due to the high DC bias close to the minimum of the optical transfer function and low modulation index for flat subcarrier generation. The amplitude of the RF signal after the first driving amplifier was duple of the half-wave voltage of the PM (PM_1) in order to generate multiple spectral subcarriers. Due to the limited amplitude of the RF signal, the peak number was limited (the peak number was 29). In order to obtain more subcarriers, we cascaded another PM (PM_2), which was driven by a high-level RF signal with fixed frequency of 25 GHz. Then, we cascaded another IM driven by the RF signal with a fixed frequency of 25 GHz. This IM was used to generate many flat optical subcarriers, thereby ensuring that every subcarrier could be modulated by transmitted information. The total output power for generated subcarriers after the IM for experiment was only 2.7 dBm.

The numerical simulated optical spectra are shown in Figs. 6(a)–(d), and the experimental results are shown in Fig. 6(e)–(h). The simulated optical spectra before and after PM_1 are shown in Figs. 6(a) and (b), respectively; meanwhile, Figs. 6(c) and d show the simulated optical spectra after PM_2 and MZM, respectively. As can be seen, when the amount of subcarriers is doubled using PM_2, the power fluctuation is worse than that of PM_1-only optical subcarriers, which can be improved by concatenated MZM as shown in Fig. 6(c). The measured spectrum of the output signal after the first PM is shown in Fig. 6(f); as can be seen, there are 25 subcarriers and a large power fluctuation of almost 60 dB. After the second PM, the number of subcarriers reached over 40 with very large peak power fluctuation as shown in Fig. 6(g). The experimental results show that over 70% of the subcarriers can be attributed to the second modulator introduced in this novel scheme. However, after the MZM, the output presents a very good performance, generating 19 subcarriers with peak power fluctuation less than 2 dB, and 28 subcarriers with peak power fluctuation less than 4 dB (Fig. 6(h)). These figures demonstrate that the experiment results have good agreement with the numerical simulated results.

In addition, a BTB transmission experiment for 100-Gb/s polarization multiplexing QPSK signal carried by the generated subcarrier was set up. Figure 7 shows the configuration of the transmission system. We used one optical filter with 3 dB bandwidth of 0.2 nm cascaded by one 12.5-GHz interleaver to select one subcarrier with the smallest tone-to-noise ratio. One EDFA was used to boost the optical power, and one polarization controller was employed to control the polarization direction before the I/Q modulator (I/Q MOD). This I/Q MOD driven by

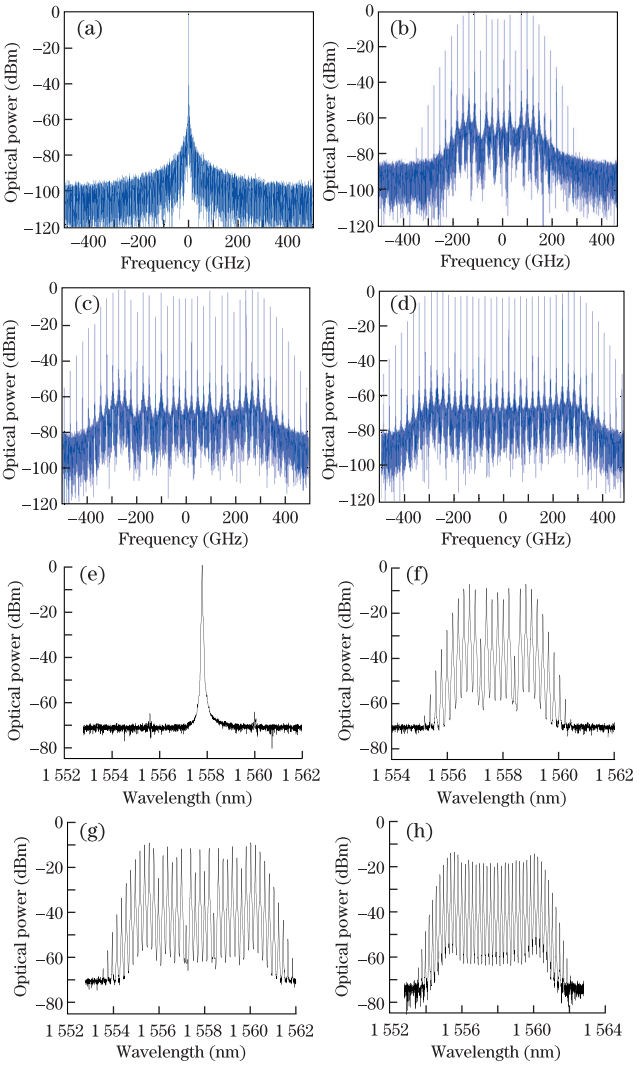

Fig. 6. Numerical simulated optical spectra (a) before PM1, and after (b) PM1, (c) PM2, and (d) IM; the experimental results of the optical spectra (e) before PM1, and after (f) PM1, (g) PM2, and (h) IM.

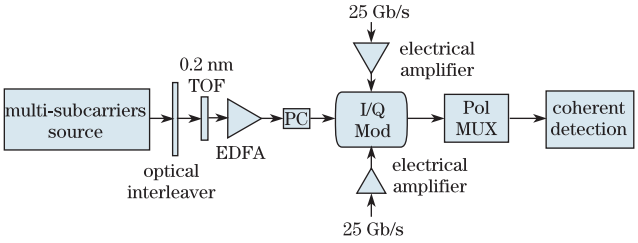

Fig. 7. Transmission experimental setup of 100-Gb/s polarization multiplexing QPSK signal generation and detection.

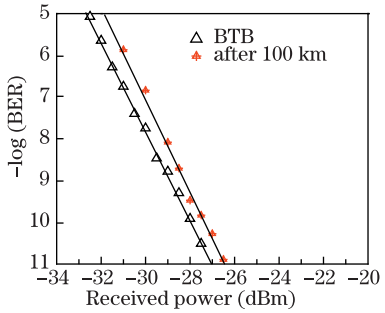

Fig. 8. BER curve verus the received power for 100-Gb/s polarization multiplexing QPSK signal.

25-Gb/s random binary sequence contained two parallel MZMs to modulate the subcarrier. After I/Q modulation, this 50-Gb/s QPSK data were polarization multiplexed through the polarization-multiplexer; afterwards, a polarization multiplex emulation by split-delay-add structure was also introduced, thus generating 100-Gb/s polarization multiplexing QPSK signal. At the receiver, an ECL with a line-width less than 100 kHz was used as the local oscillator (LO) for coherent detection. A polarization-diverse 90° hybrid was used to realize the polarization of the LO and received optical signal before balance detection. The captured data were processed through offline digital signal processing.

Figure 8 shows the BER curve versus the received power of the 100-Gb/s transmission experiment. As can be seen, in the 100-Gb/s polarization multiplexing QPSK signal, the receiver sensitivity of the BTB signal is −28.6 dBm, and the power penalty is lower than 1 dB after 100-km transmission at the BER of 1×10^{-9}. The constellation is also inserted in this figure.

In conclusion, we propose and experimentally demonstrate a scheme to generate coherent optical subcarriers with flat power spectra by cascading PMs and a MZ IM driven by same frequency sinusoidal RF sources. Theoretical analysis and numerical study are carried out on this novel scheme. We use 25-GHz RF synchronous sinusoidal signals to drive cascaded two-stage PMs and an IM to generate 28 subcarriers with peak power fluctuation less than 4 dB. The measured tone-to-noise ratio of the subcarrier is higher than 40 dB. The experiment results show that for 100-Gb/s polarization multiplexing QPSK signal, the receiver sensitivity of the BTB signal is −28.6 dBm, and the power penalty is lower than 1 dB after 100-km transmission at the BER of 1×10^{-9}. Moreover, the experimental results of the generated multi-carriers of this novel scheme compared with the other regular schemes show that it has great potential in future Tb/s communication.

This work was partially supported by the National "973" Program of China (No. 2010CB328300), the National Natural Science Foundation of China (Nos. 61107064, 61177071, and 600837004), the Doctoral Fund of Ministry of Education, the Open Fund of the State Key Lab of ASIC & System (No. 11MS009), the Pujiang Fund, and the Shuguang Fund.

References

1. R. Dischler and F. Buchali, in *Proceedings of OFC2009* PDPC2 (2009).
2. J. Yu, Z. Dong, X. Xiao, Y. Xia, S. Shi, C. Ge, W. Zhou, N. Chi, and Y. Shao, in *Proceedings of OFC 2011* PDPA6 (2011).
3. Y. Shao, N. Chi, C. Hou, W. Fang, J. Zhang, B. Huang, X. Li, S. Zou, X. Liu, X. Zheng, N. Zhang, Y. Fang, J. Zhu, L. Tao, and D. Huang, J. Lightwave Technol. **28,** 1770 (2010).
4. Y. Shao, J. Zhang, W. Fang, S. Zou, X. Li, B. Huang, N. Chi, and S. Yu, Chin. Opt. Lett. **8,** 894 (2010).
5. Y. Yang and J. Wang, IEEE Trans. Parallel Distr. Syst. **16,** 51 (2005).
6. W. Idler, E. Lach, W. Kuebart, B. Junginger, K. Schuh, A. Klekamp, D. Werner, A. G. Steffan, A. Schippel, M. Schneiders, S. Vorbeck, and R. Braun, J. Lightwave Technol. **29,** 2195 (2011).
7. J. Yu, X. Zhou, M. Huang, D. Qian, P. N. Ji, T. Wang, and P. Magill, Opt. Express **17,** 17928 (2009).
8. Y. Ma, Q. Yang, Y. Tang, S. Chen, and W. Shieh, in *Proceedings of OFC2009* PDPC1 (2009).
9. J. Armstrong, J. Lightwave Technol. **27,** 189 (2009).
10. J. Yu, Electron. Lett. **46,** 775 (2010).
11. H. Suzuki, M. Fujiwara, and K. Iwatsuki, J. Lightwave Technol. **24,** 1998 (2006).
12. H. Takara, T. Ohara, K. Mori, K. Sato, E. Yamada, Y. Inoue, T. Shibata, M. Abe, T. Morioka, and K-I. Sato, Electron. Lett. **36,** 2089 (2000).
13. K. R. Tamura, H. Kubota, and M. Nakazawa, IEEE J. Quantum Electron. **36,** 773 (2000).
14. J. J. Veselka and S. K. Korotky, IEEE Photon. Technol. Lett. **10,** 958 (1998).
15. M. Fujiwara, M. Teshima, J. Kani, H. Suzuki, N. Takachio, and K. Iwatsuki, J. Lightwave Technol. **21,** 2705 (2003).
16. R.Wu, V. R. Supradeepa, C. M. Long, D. E. Leaird, and A. M. Weiner, in *Proceedings of 2010 IEEE Topical Meeting on Microwave Photonics (MWP)* 212 (2010).
17. R. Wu, V. R. Supradeepa, C. M. Long, D. E. Leaird, and A. M. Weiner, Opt. Lett. **35,** 3234 (2010).
18. T. Kawanishi, T. Sakamoto, S. Shinada, and M. Izutsu, IEICE Electron. Express **1,** 217 (2004).
19. J. Zhang, N. Chi, J. Yu, Y. Shao, J. Zhu, B. Huang, and L. Tao, Opt. Express **19,** 17891 (2011).
20. S. Zou, Y. Shao, X. Zheng, W. Fang, X. Li, and N. Chi, Acta Opt. Sin. (in Chinese) **31,** 0706004 (2011).